320-221

Spectral Kurtosis Identification of Deep-Space Technosignatures

Gelu M Nita[1*] , Dale E. Gary[1], and Gregory Hellbourg[2]

NJIT New Jersey Institute of Technology

[1]New Jersey Institute of Technology, Newark, NJ 07102, USA
[2]International Centre for Radio Astronomy Research, Curtin University, Bentley, WA 6102, Australia
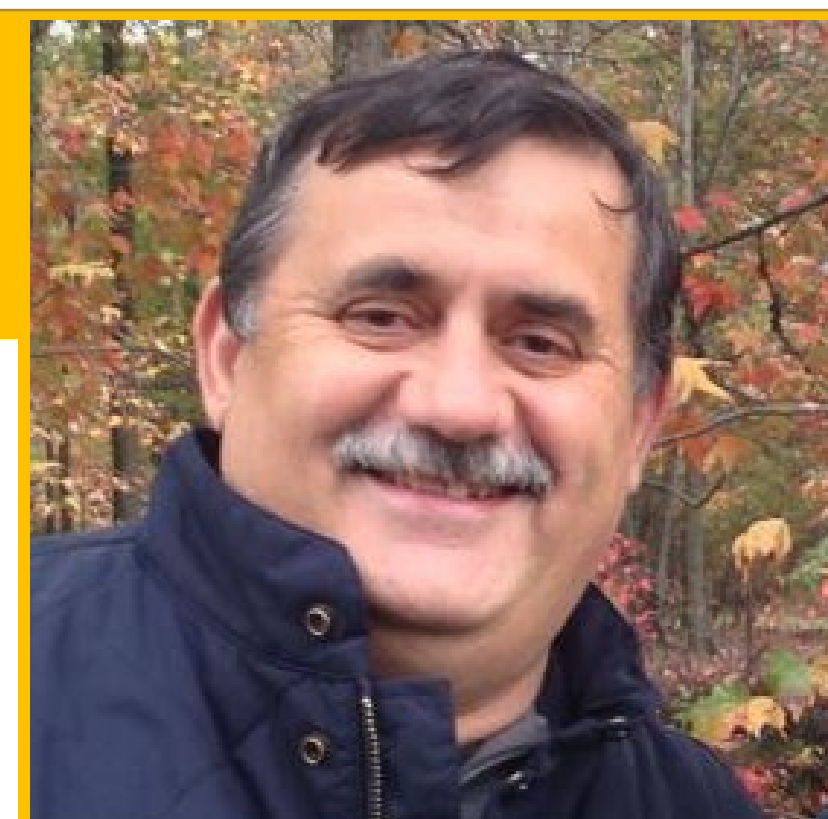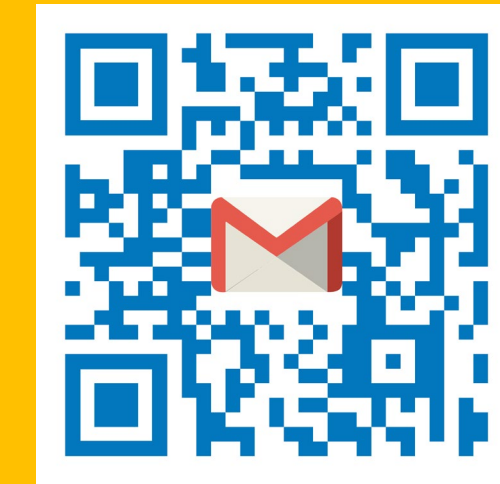
Theoretical Background: The Generalized Spectral Kurtosis Estimator

Theorem (Nita and Gary 2010a): Given a set of M-independent random variables $\{x_i\}$ sampled from a parent population described by a gamma distribution $f(x,a,d) = x^{d-1} e^{-\frac{x}{a}}/a^d \Gamma(d)$, the infinite set of statistical moments of the ratio MS_2/S_1^2, where $S_1 = \sum_{i=1}^M x_i$ and $S_1 = \sum_{i=1}^M x_i^2$, is given by the expression

$$E\left[\left(\frac{MS_2}{S_1^2}\right)^n\right] = \frac{M^n \Gamma(Md)}{\Gamma(d)^M \Gamma(Md+2n)} \times \frac{\partial^n}{\partial t^n}\left[\sum_{r=0}^n \frac{1}{r!}\Gamma(2r+d)t^r\right]^M \Bigg|_{t=0},$$

which is independent of the scale factor, a, of the underlying distribution.

Corollary: The Generalized Spectral Kurtosis Estimator, $\widehat{SK} = \frac{Md-1}{M+1}\left(\frac{MS_2}{S_1^2} - 1\right)$, has an unbiased unity expectation, $E(\widehat{SK}) = 1$, and the infinite series of the central moments of its probability distribution function (PDF), $\mu_n = E\left[(\widehat{SK}-1)^n\right]$, have closed analytical expressions involving the known, scale factor-independent, expectations $E\left[\left(\frac{MS_2}{S_1^2}\right)^n\right]$.

Practical application: If an astronomical background signal, or a numerical transformation of it, is expected to obey a gamma distribution $f(x,a,d)$, one may compute thresholds with known probabilities of false alarm (PFA) to detect a continous or transient mixture with a signal of interest obeying a different statistical distribution.

The Spectral Kurtosis Spectrometer

If the time domain samples of an astronomical signal obey a normal distribution, the Fast Fourier Transform (FFT)-based Power Spectral Density estimates (PSD) obey an exponential distribution (Gamma distribution of shape factor $d = 1$), and its contamination by man-made radio frequency interference (RFI) is indicated by deviations of the $\widehat{SK}$ estimator above or below unity, depending on the RFI duty-cycle relative to the integration time. Figure 1 illustrates the design of an FFT-based spectrograph with built-in automatic RFI detection as it has been proposed and tested by Nita et al. 2007 in a form of a software correlator and hardware-implemented in the Korean Solar Radio Burst Locator (KSRBL, Gary, Liu and Nita 2010). The recently commissioned Expanded Owens Valley Solar Array (EOVSA, Nita et al. 2016a) is the world-first radio interferometry instrument having a built-in automatic real-time RFI detection and excision engine.
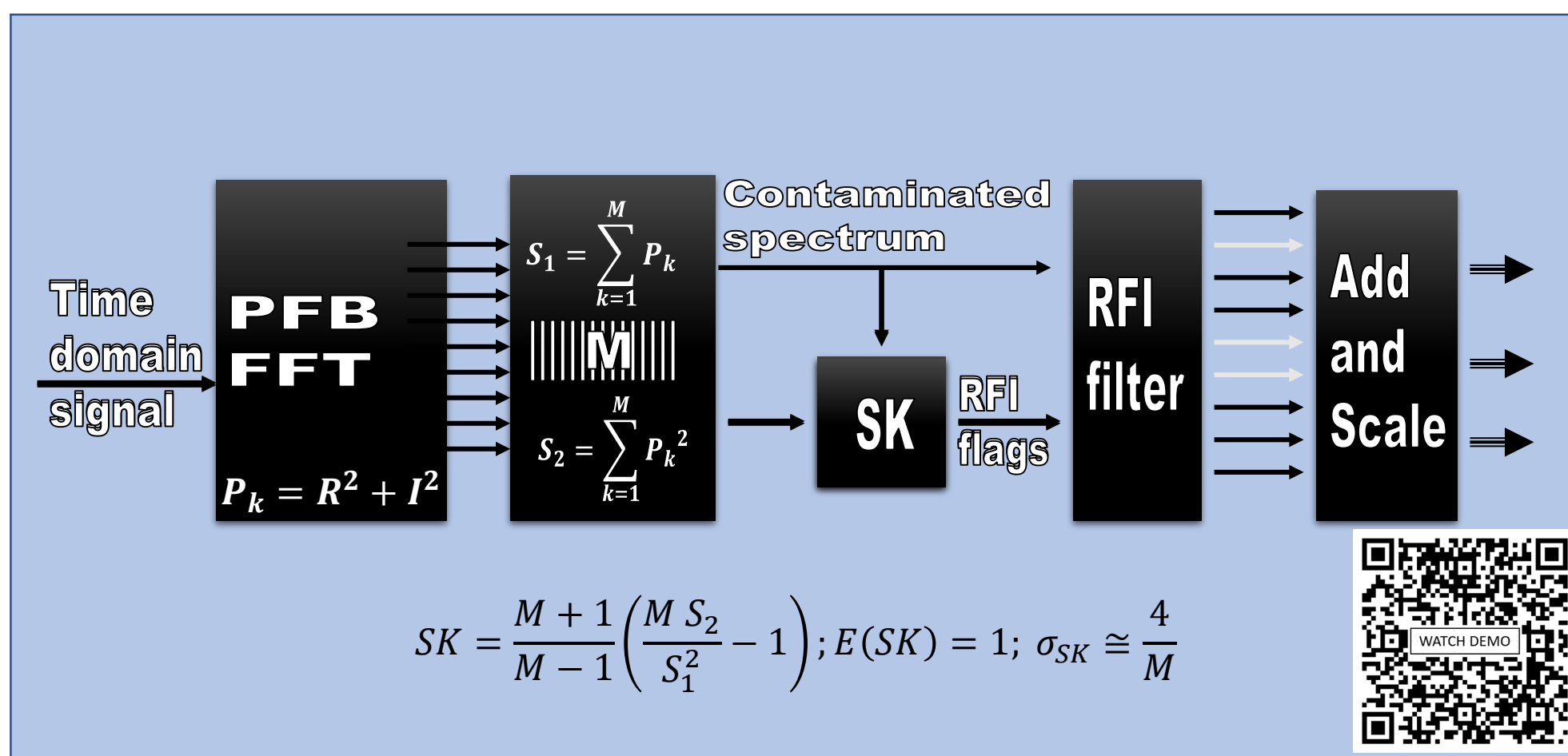

Figure 1: Schematics of the FFT-based (d=1) Spectral Kurtosis Spectrometer. Scan the embedded QR code to watch a video demonstrating SK real-time detection of cell phone-induced RFI.

Spectral Kurtosis: Not Only a RFI Detection Tool

Nita 2016 obtained analytical approximations of the expected values for the $\widehat{SK}$ estimator and its variance in the case of transient signals of artificial or astrophysical nature, as a function of their duration relative to the instrumental integration time (effective duty-cycle) and the signal to noise ratio (SNR), showing that, as illustrated in Fig. 1 left panel, the $\widehat{SK}$ estimator associated with a Gaussian transient can only deviate above unity, while the $\widehat{SK}$ estimator corresponding to artificial transients may deviate below unity for relative duty-cycles larger than 50%. As shown in the middle and right panels, this allows unambiguous statistical discrimination of the artificial and natural transients, thus, the $\widehat{SK}$ estimator may serve as a powerful signal detection and classification tool.
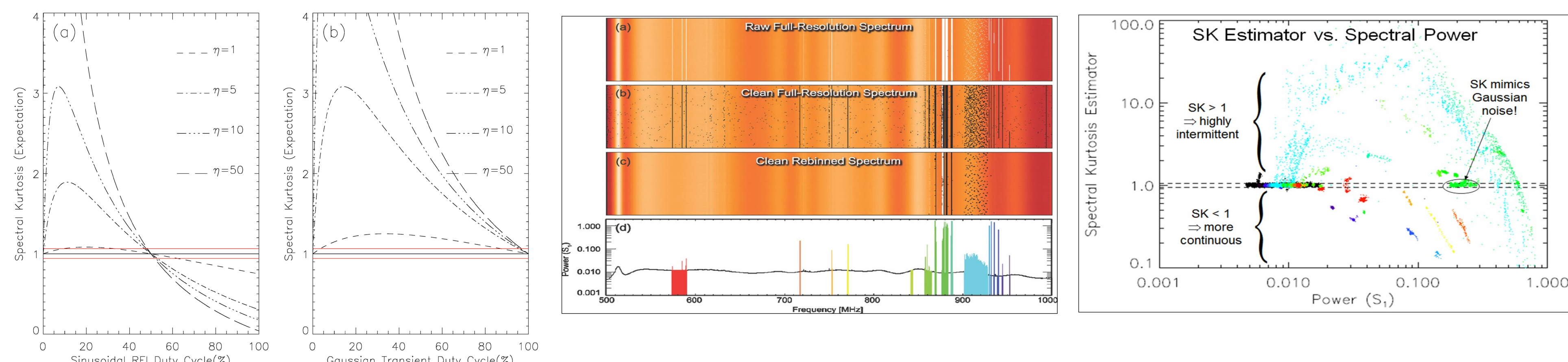

Figure 2: SK Dependence on the Duty-Cycle of RFI and Gaussian Transient Signals (Nita 2016 b). **Left panel: a)** RFI signals: SK deviates above unity for less than 50% duty-cycles (short transients), and below unity for larger than 50% duty-cycles (long transients or continous RFI) **b)** Gaussian transient signals: SK never deviates below unity. **Middle:** Dynamic and integrated spectra recorded by the KSRBL SK spectrograph (Gary et al. 2010b) featuring various types of RFI contamination. **Right:** SK-Power diagram demonstrating the SK discrimination of transient types based on their duty-cycles and statistical nature.

Multiscale Spectral Kurtosis Analysis

Nita 2016 proposed a practical data analysis pipeline design, called Multiscale Spectral Kurtosis Analysis (MSKA), which may transform an $\widehat{SK}$ spectrograph having a fixed accumulation length into a versatile system capable of unambiguous statistical classification of transients by varying the duty-cycle of the detected transient signals.
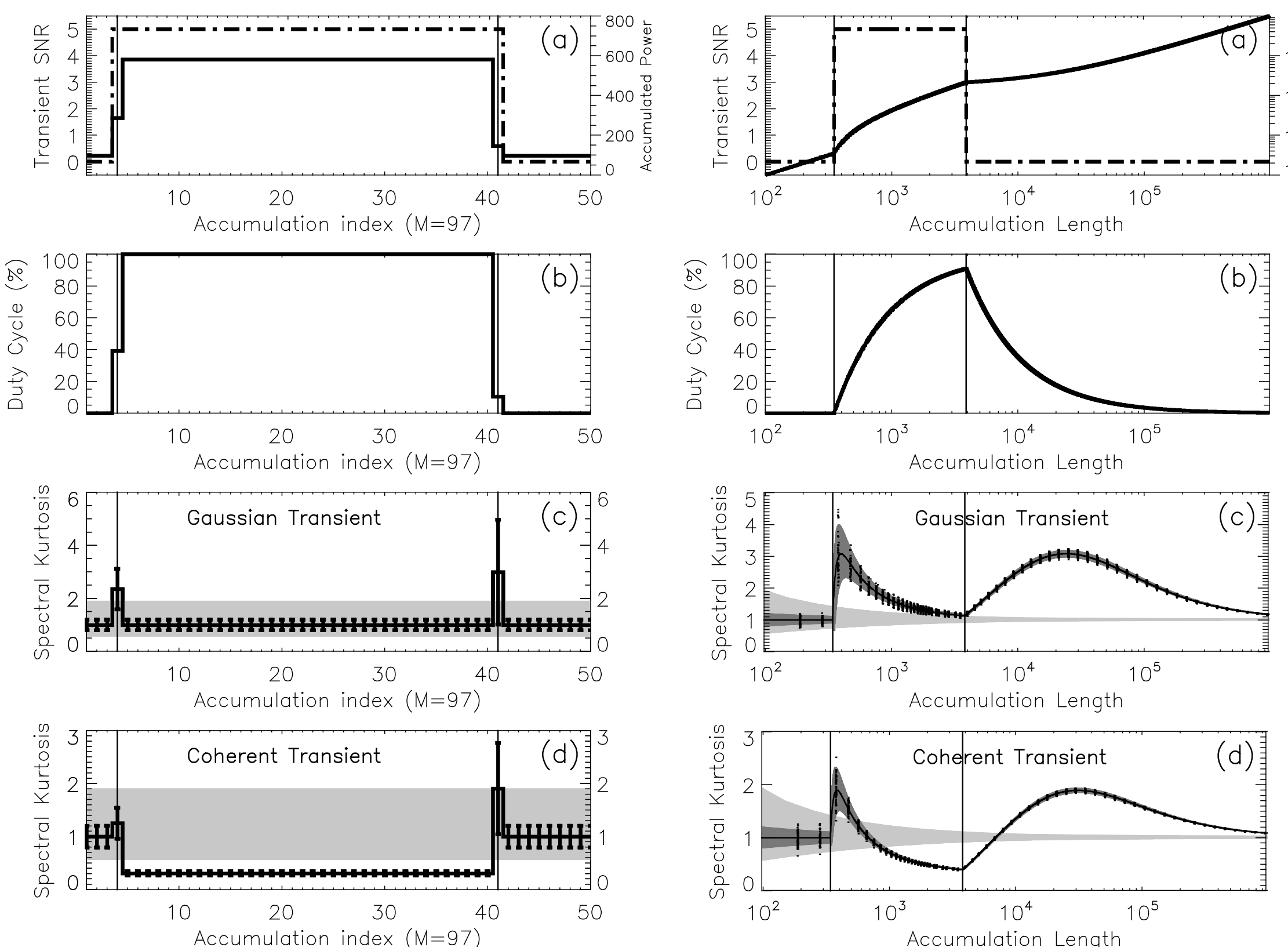

Figure 3 Left panel: Expected $\widehat{SK}$ discrimination of two transients lasting longer than the accumulation length ($M = 97$). The transients, which have different underplaying statistics, have the same duration (3540 raw FFT blocks) and SNR=5, and start at the same offset (350 raw FFT blocks) relative to the start of the first accumulation. (a) SNR (dot–dashed line) and accumulated power (solid line) as a function of the accumulation block index. b) The duty-cycle profile of both transients. $\widehat{SK}$ (solid line) and $\widehat{SK} \pm \sigma_{\widehat{SK}}$ (error bars) for the Gaussian and coherent transients are shown in panels (c) and (d), respectively. The range bounded by the 0.13% PFA detection thresholds, [0.56, 1.90], is indicated by the grey-shaded areas in panels (c) and (d). The accumulation blocks during which the transients start and end are marked by vertical lines in all panels.

Right panel: Expected $\widehat{SK}$ profiles as function of a varying accumulation length for the same pair of transients considered in the left panel. The SNR (dot–dashed line) and accumulated power (solid line) profiles are shown in panel (a), and the duty-cycle profile is shown in panel (b). A series of numerically generated $\widehat{SK}$ random variates corresponding to a set of selected integer multiples of the minimum accumulation length, $M = 97$, are overlaid (symbols) on the $\widehat{SK}$ (solid line) and $\widehat{SK} \pm \sigma_{\widehat{SK}}$ (dark shaded areas) corresponding to the Gaussian (panel c) and coherent (panel d) transients. The range bounded by the 0.13% PFA detection thresholds is indicated by the grey-shaded areas in panels (c) and (d). The start and end of the transients are marked by vertical lines in all panels.

SK Gaussian Signature of the FRB 121102 Inferred through Multiscale Spectral Kurtosis Analysis

Nita, Keipema, & Paragi 2019, 2018, using data streamed from the 305-m William E. Gordon Telescope at the Arecibo Observatory and recorded at the Joint Institute for VLBI ERIC (JIVE), unambiguously demonstrated the Gaussian nature of one of the FRB 1221102 repeating signals.
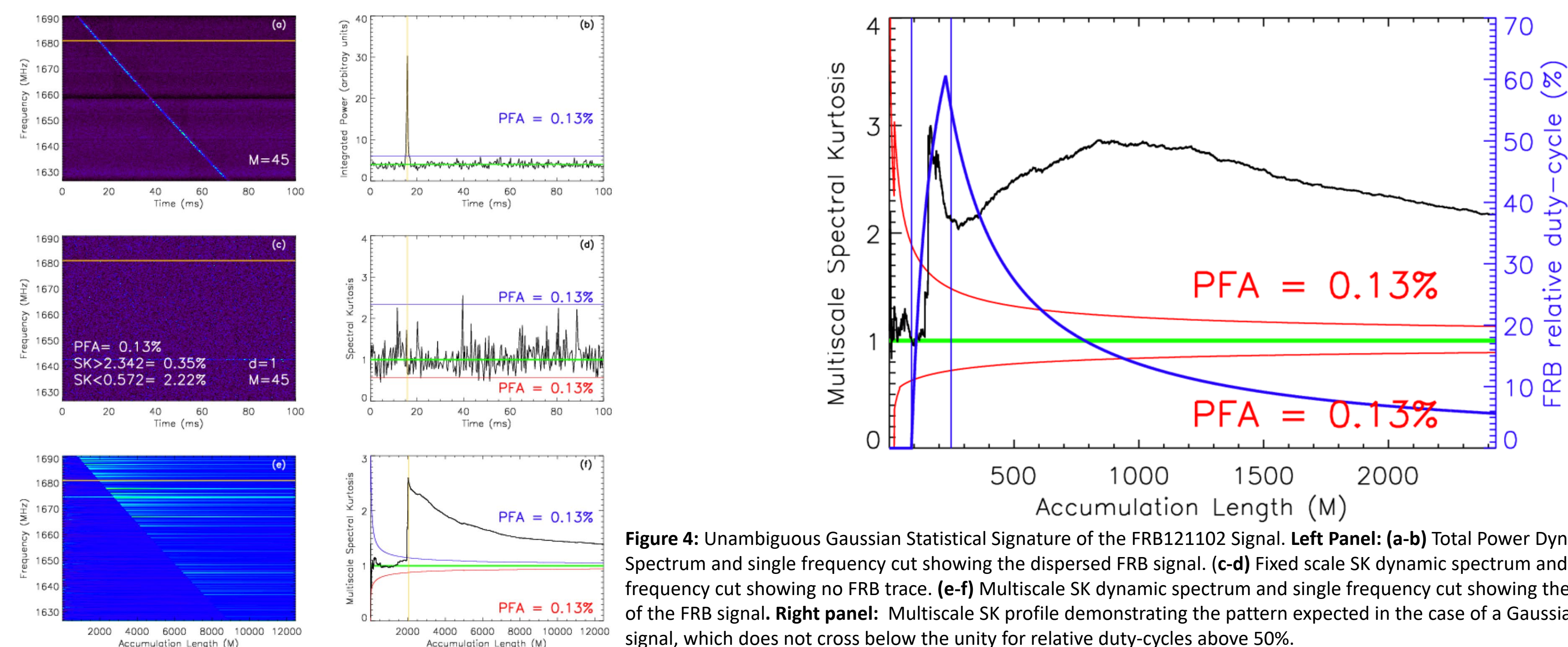

Figure 4: Unambiguous Gaussian Statistical Signature of the FRB121102 Signal. **Left Panel: (a-b)** Total Power Dynamic Spectrum and single frequency cut showing the dispersed FRB signal. **(c-d)** Fixed scale SK dynamic spectrum and single frequency cut showing no FRB trace. **(e-f)** Multiscale SK dynamic spectrum and single frequency cut showing the detection of the FRB signal. **Right panel:** Multiscale SK profile demonstrating the pattern expected in the case of a Gaussian transient signal, which does not cross below the unity for relative duty-cycles above 50%.

SK Gaussian Signature of the FRB 180301 Inferred through Bandwidth Spectral Kurtosis Analysis

Here we employ, **for the first time**, a new method of Spectral Kurtosis analysis to investigate the yet controversial nature of the FRB 180301 signal detected during the Breakthrough Listen observations with the Parkes telescope (Price et al., 2019). In this particular analysis we use coherently dedispersed data from two of a total of 44 observing 3.5 MHz-wide frequency bands, centered on 1421.8 MHz and 1414.83 MHz, respectively. To better resolve the FRB time profile, our approach is to produce FFT dynamic spectra using partially overlapping time blocks. Although the statistical independence of the PSD estimates, which is assumed by the SK theory, is violated in the time direction due to this overlapping, the PSD estimates corresponding to the same time bin remain statistically independent along the frequency axis, being constructed from a set of statistically independent time samples. This allows us to employ without any needed modifications the general theory of the SK estimator by accumulating the PSD estimates, and their squares, across the observing bandwidths, as illustrated in Figure 5, which demonstrates the distinct SK signatures of the RFI signal present in the (1421.8 ±1.75) MHz channel and the FRB pulse visible in the channel and (1414.83±1.75) MHz .
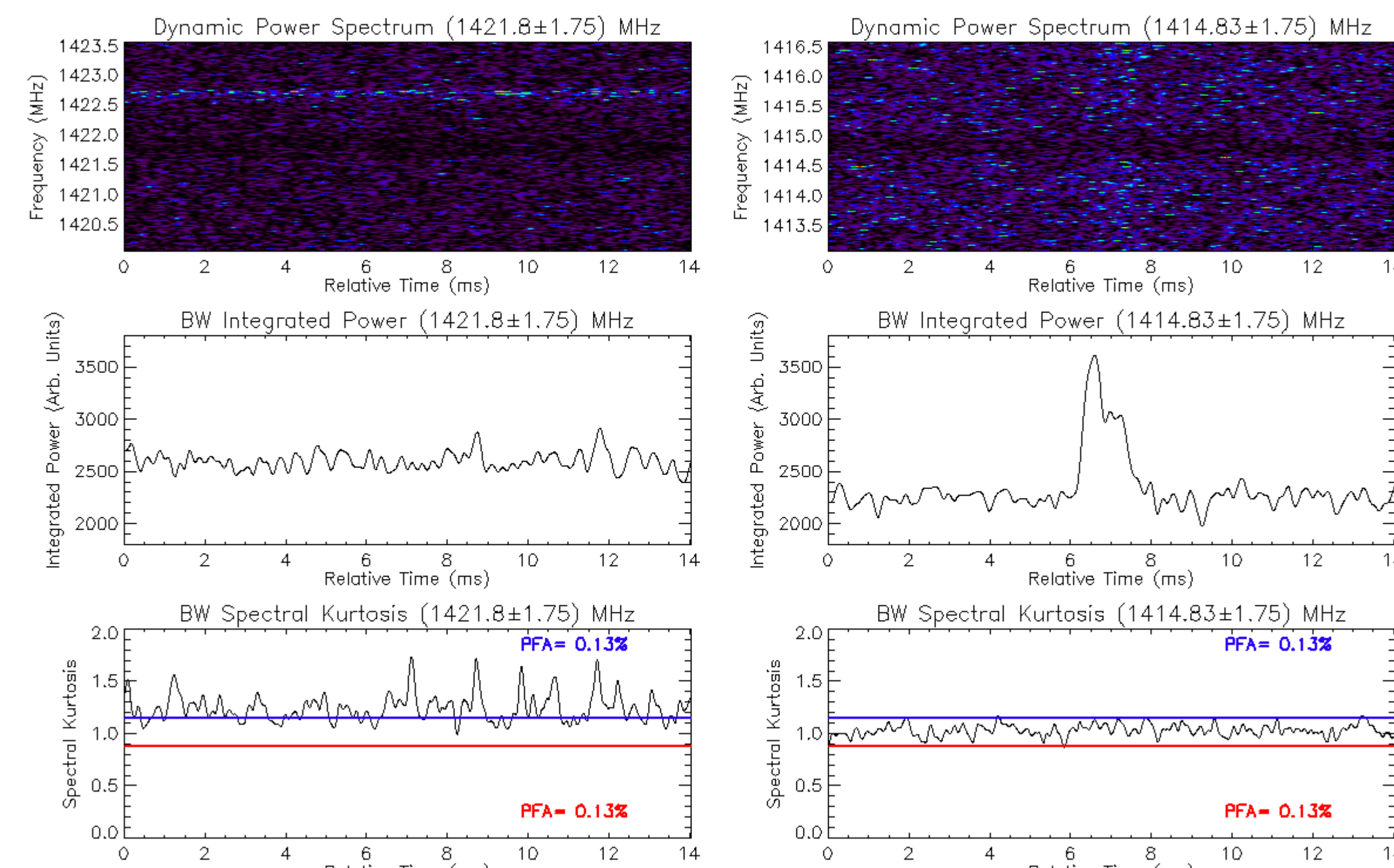

Figure 5: Bandwidth SK analysis of a data segment containing the FRB 180301 signal.

Left column, top panel: Dynamic spectrum for the (1421.8 ±1.75) MHz channel revealing a narrow band bright signal around ~1422.75 MHz.

Left column, middle panel: Bandwidth-integrated power showing no particular time variation.

Left column, bottom panel: Bandwidth-computed Spectral Kurtosis time profile consistent with the bandwidth-relative low duty-cycle of the observed narrow-band signal, which is flagged as RFI contamination by the SK upper PFA=0.13% threshold (blue horizontal line).

Right column, top panel: Dynamic spectrum for the (1414.83±1.75) MHz channel revealing relatively faint cross-band brightness enhancement between the 6 and 8 millisecond time marks relative to the start of the data segment.

Right column, middle panel: Bandwidth-integrated power confirming the presence of the FRB pulse.

Right column, bottom panel: Bandwidth-computed Spectral Kurtosis time profile showing statistical fluctuations about a constant unity mean bounded by the lower and upper PFA=0.13% threshold (red, and respectively, blue horizontal line). This result unambiguously demonstrates the Gaussian nature of the FRB 180301 signal present in the (1414.83±1.75) MHz channel.

Spectral Kurtosis Analysis of the Voyager 1 Signal

Here we investigate the SK statistical signature of a signal observed with the Robert C. Byrd Green Bank Telescope Breakthrough Listen back-end (MacMahon et al. 2018) that was transmitted by the Voyager1 spacecraft, which is up to date the only known source of artificial signals originating from outside our solar system, and we demonstrate the ability of the SK estimator to perform real-time detection and discrimination against natural astronomical transients of deep-space Voyager 1-like technological signatures of alien origin. In this case, our approach, illustrated in Figure 6, is to produce dynamic spectra of time-accumulated FFT power spectra and corresponding SK estimator dynamic spectra using different frequency and time resolutions in different duty-cycles relative to the integration time of the drifting Voyager 1 telemetry signal. Our result demonstrates that, if a larger than 50% relative duty-cycle is generated for an appropriate choice of the frequency resolution and integration length, this technique may unambiguously reveal the artificial nature of such transient signals.
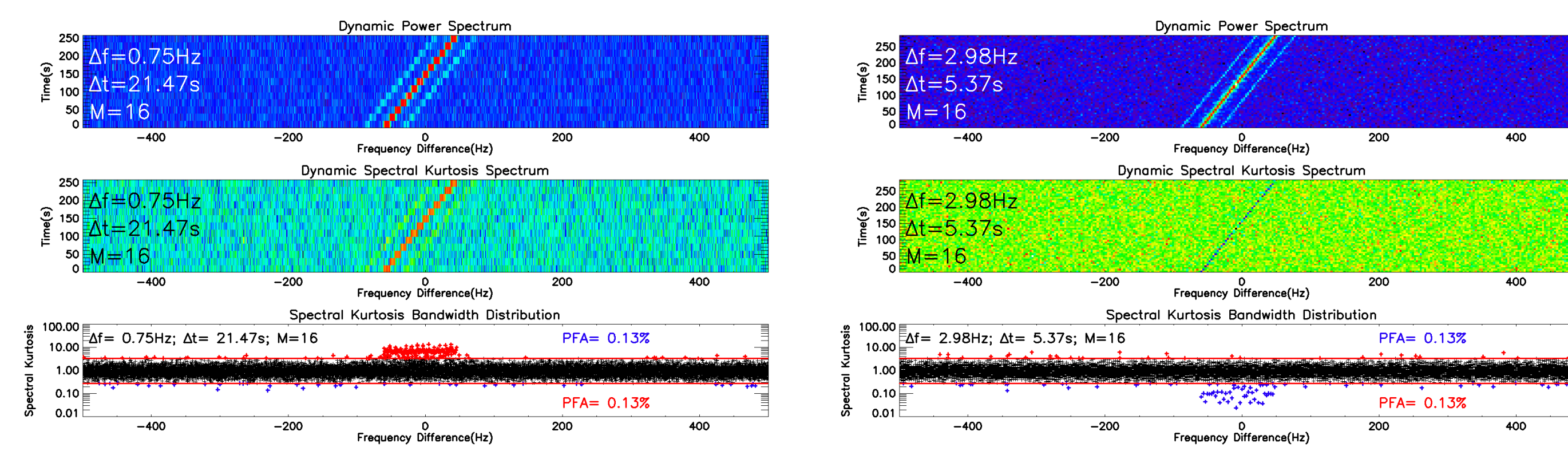

Figure 6: Multi-scale SK analysis of a Voyager 1 telemetry signal. **Top row:** Dynamic spectra of the total power accumulated over $\Delta t = 21.48s$ (left panel) and $\Delta t = 5.37s$ (right panel). The frequency resolutions o f $\Delta f = 0.75Hz$ and $\Delta f = 2.98Hz$, respectively, were chosen such as the accumulation length is M=16 in both cases. **Middle Row:** SK dynamic spectra showing the traces of the drifting telemetry signal.

Bottom row: SK bandwidth distributions showing statistically significant, duty-cycle-dependent, deviations above and below unity (respectively red and blue symbols) of the Voyager 1 SK values.

References

1. Gary, D. E., Liu, Z., & Nita, G. M. 2010, PASP, 122, 560, doi: 10.1086/652410
2. Kar, A., Kuske, A., Hawkins, L., Prestage, R., & Smith, E. 2019, in American Astronomical Society Meeting Abstracts, Vol. 233, American Astronomical Society Meeting Abstracts #233, #152.01
3. Lorimer, D. R., Bailes, M., McLaughlin, M. A., Narkevic D. J., & Crawford, F. 2007, Science, 318, 777, doi:10.1126/science.1147532
4. MacMahon, D. H., Price, D. C., Lebofsky, M., et al. 2018, PASP, 130, 044502
5. Nita, G. M. 2016, MNRAS, 458, 2530, doi:10.1093/mnras/stw550
6. Nita, G. M., & Gary, D. E. 2010a, PASP, 122, 595
7. —. 2010b, MNRAS, 406, L60, doi: 10.1111/j.1745-3933.2010.00882.x
8. Nita, G. M., Gary, D. E., & Hellbourg, G. 2016a, in 2016 Radio Frequency Interference (RFI), 75–80
9. Nita, G. M., Gary, D. E., Liu, Z., Hurford, G. J., & White, S. M. 2007, PASP, 119, 805, doi: 10.1086/520938
10. Nita, G. M., Hickish, J., MacMahon, D., & Gary, D. E. 2016b, JAI, 5, 1641009, doi: 10.1142/S2251171716410099
11. Nita, G. M., Keimpema, A., & Paragi, Z. 2018, http://sigport.org/3682
12. —. 2019, JAI, 1, doi: 10.1142/S2251171719400087
13. Price, D. C., Foster, G., Geyer, M., et al. 2019, arXiv eprints. https://arxiv.org/abs/1901.07412
14. Scholz, P., Spitler, L. G., Hessels, J. W. T., et al. 2016, ApJ, 833, 177, doi: 10.3847/1538-4357/833/2/177
15. Spitler, L. G., Scholz, P., Hessels, J. W. T., et al. 2016, Nature, 531, 202, doi: 10.1038/nature17168
16. Taylor, J., Denman, N., Bandura, K., et al. 2019, JAI, 1, doi: 10.1142/S2251171719400004X